J. Sci. Univ. Kelaniya 18 (2) (2025): 191-202 https://doi.org/10.4038/josuk.v18i2.8167

Study of Demagnetization Energy in FCC Ferromagnetic Thin Films with Two Spin Layers Using the Fourth-Order Perturbed Heisenberg Model

M.S.M. Farhan[1*] and P. Samarasekara[2]

[1]Department of Physical Science, Trincomalee Campus, Eastern University, Sri Lanka.
[2]Department of Physics, University of Peradeniya, Peradeniya, Sri Lanka.

*****Corresponding author: farhanmsm@esn.ac.lk

ORCID ID: https://orcid.org/0009-0001-8708-9460

Received: 29.05.2025 Revised: 28.10.2025 Accepted: 31.10.2025 Online: 15.12.2025

Abstract This research explores the magnetic behaviour of ferromagnetic thin films with a face-centred cubic (FCC) structure using the fourth-order perturbed Heisenberg Hamiltonian. By incorporating all key magnetic energy parameters, including spin exchange interactions, anisotropy constants, applied magnetic fields, stress-induced anisotropy, and demagnetization energy, a comprehensive analysis of the energy landscape in FCC thin films is provided. MATLAB simulations generate 3D and 2D plots, highlighting the influence of higher-order anisotropy terms on magnetic energy distribution, and revealing distinct energy maxima and minima. The results show that the total magnetic energy in the demagnetization model is lower compared to the stress-induced model, suggesting that internal stress plays a significant role in enhancing the system's energy state. Additionally, the study reveals deviations from the conventional 90-degree separation between magnetic easy and hard axes, indicating the complex interplay of anisotropy and spin interactions. The exchange of fourth-order anisotropy constants between the two spin layers also subtly influences the energy landscape, emphasizing the importance of anisotropy distribution in system stability. These findings contribute valuable insights for optimizing the magnetic properties of ferromagnetic thin films in spintronic applications, data storage, and other advanced magnetic materials. Future research could extend the analysis to multilayered structures and higher perturbation orders to refine the theoretical framework for thin-film magnetism.

Keywords: Demagnetization energy, Fourth order perturbed Heisenberg Hamiltonian, Magnetic anisotropy constant, Magnetic thin films, Spin layers.

Introduction

Ferromagnetic thin films have gained significant attention in condensed matter physics due to their critical applications in spintronics, data storage, and sensor technologies. Understanding the magnetic properties of these films is essential for optimizing their performance in advanced technological applications. One of the most effective theoretical approaches for studying the magnetic behaviour of ferromagnetic thin films is the Heisenberg Hamiltonian model, which accounts for spin interactions at the atomic level. Higher-order perturbations of this model, particularly the fourth-order perturbed Heisenberg Hamiltonian, provide deeper insights into the energy landscape of magnetic systems by incorporating all seven key magnetic energy parameters. These parameters include spin exchange interaction, second-order anisotropy constants, fourth-order anisotropy constants, in-plane and out-of-plane applied magnetic field, stress induced anisotropy constants, and demagnetization energy.

Several theoretical models and computational methods have been employed in previous research to investigate the magnetic properties of ferromagnetic thin films. For example, Monte Carlo simulations have been applied to study magnetic hysteresis in thin films deposited on specialized substrates, providing valuable insights into the response of magnetization under external magnetic fields (Zhao et al., 2002). The Ising model has also been widely used to explore the spin interactions in multilayered thin films with alternating structures, highlighting important characteristics of their magnetic behaviour (Bentaleb et al., 2002). Additionally, first-principles band structure calculations have been utilized to examine the structural and magnetic properties of two-dimensional FeCo alloys, offering a deeper understanding of their electronic and spin-dependent features (Spisak & Hafner, 2005). Similarly, the Korringa-Kohn-Rostoker Green's function method has been employed to investigate the magnetic behaviour of nickel layers deposited on copper, revealing critical details about interfacial magnetism and electronic interactions (Ernst et al., 2000).

In this study, we investigate the magnetic properties of face-cantered cubic (FCC) structured ferromagnetic thin films with two spin layers using the fourth-order perturbed Heisenberg Hamiltonian. Previous studies on simple cubic (SC) and body-centred cubic (BCC) structures have demonstrated that higher-order anisotropy terms significantly influence the magnetic energy distribution (Farhan & Samarasekara, 2022; Farhan et al., 2023; Farhan et al., 2024). The second-order perturbed Heisenberg Hamiltonian, incorporating spin exchange interactions, long-range dipole interactions, and second-order magnetic anisotropy, has been successfully applied to study the magnetic properties of ferromagnetic and ferrite thin films using a similar approach (Hucht & Usadel, 1997; Hucht & Usadel, 1999; Usadel & Hucht, 2002). Advancements in this field have extended the analysis to the third-order perturbed Heisenberg Hamiltonian, further enhancing the understanding of thin-film magnetism (Samarasekara, 2007; Samarasekara & Mendoza, 2010). Our previous work has contributed to this research by employing both second- and third-order perturbed Heisenberg Hamiltonians to investigate ferromagnetic and ferrite thin films (Samarasekara & De Silva, 2007; Samarasekara et al., 2009; Samarasekara & Warnakulasooriya, 2016). Additionally, we have determined the spin reorientation temperature of strontium ferrite thin films using the Heisenberg Hamiltonian, offering valuable insights into their temperature-dependent magnetic behaviour (Samarasekara & Saparamadu, 2013).

We focus on the relationship between the total magnetic energy, demagnetization energy, and azimuthal spin angle, which are critical factors in determining the stability and behaviour of the thin films. Utilizing MATLAB simulations, we generate both 3D and 2D plots to visualize how energy varies with changes in demagnetization energy and spin configurations. These simulations provide insights into energy maxima and minima, periodic variations in energy, and the overall stability of the ferromagnetic film.

A key aspect of our research is comparing the energy profiles of FCC-structured films with those of SC and BCC structures. By interchanging the fourth-order anisotropy constants of the two spin layers, we analyse how these modifications affect the total magnetic energy and stability of the system. The study also explores the angular dependence of energy extrema, highlighting deviations from conventional 90-degree separations between magnetic easy and hard axes.

The findings of this research contribute to a more refined understanding of the energy landscape in FCC ferromagnetic thin films. By incorporating a fourth-order perturbation model and considering all relevant energy parameters, we provide a more accurate representation of the system's magnetic behaviour. These insights have implications for the design and optimization of ferromagnetic materials in next-generation spintronic and magnetic storage applications. The results also establish a basis for further exploration of higher-order anisotropy effects in complex magnetic systems.

In the subsequent sections, we present a detailed analysis of the simulation results, followed by discussions on their implications for material stability and technological applications.

MODEL

The Heisenberg Hamiltonian for ferromagnetic thin films is expressed as follows (Samarasekara, 2007; Samarasekara & Mendoza, 2010; Samarasekara & De Silva, 2007; Samarasekara et al., 2009).

$$H = -\frac{J}{2}\sum_{m,n}\vec{S}_m.\vec{S}_n + \frac{\omega}{2}\sum_{m\neq n}\left(\frac{\vec{S}_m.\vec{S}_n}{r_{mn}^3} - \frac{3(\vec{S}_m.\vec{r}_{mn})(\vec{r}_{mn}.\vec{S}_n)}{r_{mn}^5}\right) - \sum_m D_{\lambda_m}^{(2)}(S_m^z)^2 - \sum_m D_{\lambda_m}^{(4)}(S_m^z)^4$$

$$-\sum_{\boldsymbol{m,n}}[\vec{\boldsymbol{H}} - (\boldsymbol{N_d}\vec{\boldsymbol{S}}_{\boldsymbol{n}}/\boldsymbol{\mu_0})].\vec{\boldsymbol{S}}_{\boldsymbol{m}} - \sum_{\boldsymbol{m}}\boldsymbol{K_s\, sin\, 2\theta_m} \quad (\mathbf{1})$$

In this context, $\vec{S}_m$ and $\vec{S}_n$ represent two spin vectors. The given equation can be further simplified into the following form.

$$E(\theta) = -\frac{1}{2}\sum_{m,n=1}^{N}\left[\left(JZ_{|m-n|} - \frac{\omega}{4}\Phi_{|m-n|}\right)\cos(\theta_m - \theta_n) - \frac{3\omega}{4}\Phi_{|m-n|}\cos(\theta_m + \theta_n)\right]$$

$$-\sum_{m=1}^{N}(D_m^{(2)}cos^2\theta_m + D_m^{(4)}cos^4\theta_m + H_{in}sin\theta_m + H_{out}cos\theta_m) + \sum_{m,n=1}^{N}\frac{N_d}{\mu_0}cos(\theta_m - \theta_n)$$

$$-K_s\sum_{m=1}^{N}sin2\theta_m \quad (2)$$

The spin configuration is assumed to be slightly misaligned, meaning that individual spins deviate slightly from a central average angle, denoted as θ. The azimuthal angles can therefore be expressed as:

$$\theta_m = \theta + \varepsilon_m \text{ and } \theta_n = \theta + \varepsilon_n \quad (3)$$

where ε_m and ε_n are represent small angular variations, either positive or negative. Consequently, the difference and sum of these angles are given by:

$$\theta_m - \theta_n = \varepsilon_m - \varepsilon_n \text{ and } \theta_m + \theta_n = 2\theta + \varepsilon_m + \varepsilon_n \quad (4)$$

By incorporating equations (3) and (4) into the classical Heisenberg Hamiltonian (2), we obtain the following result:

$$E(\theta) = -\frac{1}{2}\sum_{m,n=1}^{N}\left[\left(JZ_{|m-n|} - \frac{\omega}{4}\Phi_{|m-n|}\right)\cos(\varepsilon_m - \varepsilon_n) - \frac{3\omega}{4}\Phi_{|m-n|}\cos(2\theta + \varepsilon_m + \varepsilon_n)\right]$$

$$-\sum_{m=1}^{N}(D_m^{(2)}cos^2(\theta + \varepsilon_m) + D_m^{(4)}cos^4(\theta + \varepsilon_m) + H_{in}sin(\theta + \varepsilon_m)$$

$$+H_{out}cos(\theta + \varepsilon_m)) + \sum_{m,n=1}^{N}\frac{N_d}{\mu_0}cos(\varepsilon_m - \varepsilon_n) - K_s\sum_{m=1}^{N}sin2(\theta + \varepsilon_m) \quad (5)$$

The sine and cosine terms can be expressed as a series expansion, including terms up to the fourth order in ε_m and ε_n, as shown below.

$$E(\theta) = E_0 + E(\varepsilon) + E(\varepsilon^2) + E(\varepsilon^3) + E(\varepsilon^4) \quad (6)$$

Here,

$$E_0 = -\frac{1}{2}\sum_{m,n=1}^{N}\left(JZ_{|m-n|} - \frac{\omega}{4}\Phi_{|m-n|}\right) + \frac{3\omega}{8}cos2\theta\sum_{m,n=1}^{N}\Phi_{|m-n|} - cos^2\theta\sum_{m=1}^{N}D_m^{(2)}$$
$$-cos^4\theta\sum_{m=1}^{N}D_m^{(4)} - N(H_{in}sin\theta + H_{out}cos\theta + K_s sin2\theta) + \frac{N_d N^2}{\mu_0} \quad (7)$$

$$E(\varepsilon) = -\frac{3\omega}{8}sin2\theta\sum_{m,n=1}^{N}\Phi_{|m-n|}(\varepsilon_m + \varepsilon_n) + sin2\theta\sum_{m=1}^{N}D_m^{(2)}\varepsilon_m + 2cos^2\theta sin2\theta\sum_{m=1}^{N}D_m^{(4)}\varepsilon_m$$
$$-H_{in}cos\theta\sum_{m=1}^{N}\varepsilon_m + H_{out}sin\theta\sum_{m=1}^{N}\varepsilon_m - 2K_s cos2\theta\sum_{m=1}^{N}\varepsilon_m \quad (8)$$

$$E(\varepsilon^2) = \frac{1}{4}\sum_{m,n=1}^{N}\left(JZ_{|m-n|} - \frac{\omega}{4}\Phi_{|m-n|}\right)(\varepsilon_m - \varepsilon_n)^2 - \frac{3\omega}{16}cos2\theta\sum_{m,n=1}^{N}\Phi_{|m-n|}(\varepsilon_m + \varepsilon_n)^2$$
$$+cos2\theta\sum_{m=1}^{N}D_m^{(2)}\varepsilon_m^2 + 2cos^2\theta(cos^2\theta - 3sin^2\theta)\sum_{m=1}^{N}D_m^{(4)}\varepsilon_m^2 + \frac{H_{in}}{2}sin\theta\sum_{m=1}^{N}\varepsilon_m^2$$
$$+\frac{H_{out}}{2}cos\theta\sum_{m=1}^{N}\varepsilon_m^2 - \frac{N_d}{2\mu_0}\sum_{m,n=1}^{N}(\varepsilon_m - \varepsilon_n)^2 + 2K_s sin2\theta\sum_{m=1}^{N}\varepsilon_m^2 \quad (9)$$

$$E(\varepsilon^3) = \frac{\omega}{16}sin2\theta\sum_{m,n=1}^{N}\Phi_{|m-n|}(\varepsilon_m + \varepsilon_n)^3 - \frac{4}{3}sin\theta cos\theta\sum_{m=1}^{N}D_m^{(2)}\varepsilon_m^3$$
$$-4sin\theta cos\theta\left(\frac{5}{3}cos^2\theta - sin^2\theta\right)\sum_{m=1}^{N}D_m^{(4)}\varepsilon_m^3 + \frac{H_{in}}{6}cos\theta\sum_{m=1}^{N}\varepsilon_m^3 - \frac{H_{out}}{6}sin\theta\sum_{m=1}^{N}\varepsilon_m^3$$
$$+\frac{4}{3}K_s cos2\theta\sum_{m=1}^{N}\varepsilon_m^3 \quad (10)$$

$$E(\varepsilon^4) = -\frac{1}{48}\sum_{m,n=1}^{N}\left(JZ_{|m-n|} - \frac{\omega}{4}\Phi_{|m-n|}\right)(\varepsilon_m - \varepsilon_n)^4 + \frac{\omega}{64}cos2\theta\sum_{m,n=1}^{N}\Phi_{|m-n|}(\varepsilon_m + \varepsilon_n)^4$$
$$-\frac{1}{3}cos2\theta\sum_{m=1}^{N}D_m^{(2)}\varepsilon_m^4 - \left(\frac{5}{3}cos^4\theta - 8cos^2\theta sin^2\theta + sin^4\theta\right)\sum_{m=1}^{N}D_m^{(4)}\varepsilon_m^4$$
$$-\frac{H_{in}}{24}sin\theta\sum_{m=1}^{N}\varepsilon_m^4 - \frac{H_{out}}{24}cos\theta\sum_{m=1}^{N}\varepsilon_m^4 + \frac{N_d}{24\mu_0}\sum_{m,n=1}^{N}(\varepsilon_m - \varepsilon_n)^4$$
$$-\frac{2}{3}K_s sin2\theta\sum_{m=1}^{N}\varepsilon_m^4 \quad (11)$$

In the case of films containing two spin layers, *N* is equal to 2. Consequently, the values of *m* and *n* range from 1 to 2.

$$E_0 = -JZ_0 + \frac{\omega}{4}\Phi_0 - JZ_1 + \frac{\omega}{4}\Phi_1 + \frac{3\omega}{4}cos2\theta(\Phi_0 + \Phi_1) - cos^2\theta\left(D_1^{(2)} + D_2^{(2)}\right) - cos^4\theta\left(D_1^{(4)} + D_2^{(4)}\right)$$
$$-2(H_{in}sin\theta + H_{out}cos\theta + K_s sin2\theta) + \frac{4N_d}{\mu_0} \quad (12)$$

$$E(\varepsilon) = -\frac{3\omega}{4}sin2\theta[(\Phi_0 + \Phi_1)(\varepsilon_1 + \varepsilon_2)] + sin2\theta\left(D_1^{(2)}\varepsilon_1 + D_2^{(2)}\varepsilon_2\right)$$
$$+ 2cos^2\theta sin2\theta\left(D_1^{(4)}\varepsilon_1 + D_2^{(4)}\varepsilon_2\right)$$

$$-H_{in}cos\theta(\varepsilon_1+\varepsilon_2) + H_{out}sin\theta(\varepsilon_1+\varepsilon_2) - 2K_s cos2\theta(\varepsilon_1+\varepsilon_2) \quad (13)$$

$$E(\varepsilon^2) = \frac{1}{2}\left(JZ_1 - \frac{\omega}{4}\Phi_1\right)(\varepsilon_1-\varepsilon_2)^2 - \frac{3\omega}{8}cos2\theta[2\Phi_0(\varepsilon_1{}^2+\varepsilon_2{}^2)+\Phi_1(\varepsilon_1+\varepsilon_2)^2] + cos2\theta\left(D_1^{(2)}\varepsilon_1{}^2 + D_2^{(2)}\varepsilon_2{}^2\right) + 2cos^2\theta(cos^2\theta - 3sin^2\theta)\left(D_1^{(4)}\varepsilon_1{}^2 + D_2^{(4)}\varepsilon_2{}^2\right) + \frac{H_{out}}{2}cos\theta(\varepsilon_1{}^2+\varepsilon_2{}^2) - \frac{N_d}{\mu_0}(\varepsilon_1-\varepsilon_2)^2 + 2K_s sin2\theta(\varepsilon_1{}^2+\varepsilon_2{}^2) \quad (14)$$

$$E(\varepsilon^3) = \frac{\omega}{8}sin2\theta[4\Phi_0(\varepsilon_1{}^3+\varepsilon_2{}^3)+\Phi_1(\varepsilon_1+\varepsilon_2)^3] - \frac{4}{3}sin\theta cos\theta\left(D_1^{(2)}\varepsilon_1{}^3 + D_2^{(2)}\varepsilon_2{}^3\right) - 4sin\theta cos\theta\left(\frac{5}{3}cos^2\theta - sin^2\theta\right)\left(D_1^{(4)}\varepsilon_1{}^3 + D_2^{(4)}\varepsilon_2{}^3\right) + \frac{H_{in}}{6}cos\theta(\varepsilon_1{}^3+\varepsilon_2{}^3) - \frac{H_{out}}{6}sin\theta(\varepsilon_1{}^3+\varepsilon_2{}^3) + \frac{4}{3}K_s cos2\theta(\varepsilon_1{}^3+\varepsilon_2{}^3) \quad (15)$$

$$E(\varepsilon^4) = -\frac{1}{24}\left(JZ_1 - \frac{\omega}{4}\Phi_1\right)(\varepsilon_1-\varepsilon_2)^4 + \frac{\omega}{32}cos2\theta[8\Phi_0(\varepsilon_1{}^4+\varepsilon_2{}^4)+\Phi_1(\varepsilon_1+\varepsilon_2)^4] - \frac{1}{3}cos2\theta\left(D_1^{(2)}\varepsilon_1{}^4 + D_2^{(2)}\varepsilon_2{}^4\right) - (\frac{5}{3}cos^4\theta - 8cos^2\theta sin^2\theta + sin^4\theta)\left(D_1^{(4)}\varepsilon_1{}^4 + D_2^{(4)}\varepsilon_2{}^4\right) - \frac{H_{in}}{24}sin\theta(\varepsilon_1{}^4+\varepsilon_2{}^4) - \frac{H_{out}}{24}cos\theta(\varepsilon_1{}^4+\varepsilon_2{}^4) + \frac{N_d}{12\mu_0}(\varepsilon_1-\varepsilon_2)^4 - \frac{2}{3}K_s sin2\theta(\varepsilon_1{}^4+\varepsilon_2{}^4) \quad (16)$$

The first-order perturbation term can be represented as a matrix, structured in row and column form, with each containing all seven terms as follows.

$$E(\varepsilon) = \vec{\alpha}.\vec{\varepsilon} \quad (17)$$

Here terms of α are given by α_1 and α_2 .

$$\alpha_1 = -\frac{3\omega}{4}sin2\theta(\Phi_0+\Phi_1) + sin2\theta D_1^{(2)} + 2cos^2\theta sin2\theta D_1^{(4)} - H_{in}cos\theta + H_{out}sin\theta - 2K_s cos2\theta \quad (18)$$

$$\alpha_2 = -\frac{3\omega}{4}sin2\theta(\Phi_0+2\Phi_1) + sin2\theta D_2^{(2)} + 2cos^2\theta sin2\theta D_2^{(4)} - H_{in}cos\theta + H_{out}sin\theta - 2K_s cos2\theta \quad (19)$$

The second-order perturbation term can be represented using a two-by-two matrix, consisting of a row matrix and a column matrix, as shown below.

$$E(\varepsilon^2) = \frac{1}{2}\vec{\varepsilon}.C.\vec{\varepsilon} \quad (20)$$

The elements of the 2×2 matrix *C* are defined as follows.

$$C_{11} = JZ_1 - \frac{\omega}{4}\Phi_1 - \frac{3\omega}{4}cos2\theta(2\Phi_0+\Phi_1) + 2cos2\theta D_1^{(2)} + 4cos^2\theta(cos^2\theta - 3sin^2\theta)D_1^{(4)} + H_{in}sin\theta + H_{out}cos\theta - \frac{2N_d}{\mu_0} + 4K_s sin2\theta \quad (21)$$

$$C_{12} = C_{21} = -JZ_1 + \frac{\omega}{4}\Phi_1 - \frac{3\omega}{4}cos2\theta\Phi_1 + \frac{2N_d}{\mu_0} \quad (22)$$

$$C_{22} = JZ_1 - \frac{\omega}{4}\Phi_1 - \frac{3\omega}{4}cos2\theta(2\Phi_0 + \Phi_1) + 2cos2\theta D_2^{(2)} + 4cos^2\theta(cos^2\theta - 3sin^2\theta)D_2^{(4)}$$
$$+H_{in}sin\theta + H_{out}cos\theta - \frac{2N_d}{\mu_0}$$
$$+ 4K_s sin2\theta \tag{23}$$

The third-order perturbation term can be represented using a 2×2 matrix, structured as a row matrix and a corresponding column matrix, as shown below.

$$E(\varepsilon^3) = \varepsilon^2.\beta.\vec{\varepsilon} \tag{24}$$

The components of the 2×2 matrix (β) are defined by the following elements.

$$\beta_{11} = \frac{\omega}{8}sin2\theta(4\Phi_0 + \Phi_1) - \frac{4}{3}sin\theta cos\theta D_1^{(2)} - 4sin\theta cos\theta\left(\frac{5}{3}cos^2\theta - sin^2\theta\right)D_1^{(4)} + \frac{H_{in}}{6}cos\theta$$
$$-\frac{H_{out}}{6}sin\theta$$
$$+\frac{4}{3}K_s cos2\theta \tag{25}$$

$$\beta_{12} = \beta_{21}$$
$$= \frac{3\omega}{8}sin2\theta\Phi_1 \tag{26}$$

$$\beta_{22} = \frac{\omega}{8}sin2\theta(4\Phi_0 + \Phi_1) - \frac{4}{3}sin\theta cos\theta D_2^{(2)} - 4sin\theta cos\theta\left(\frac{5}{3}cos^2\theta - sin^2\theta\right)D_2^{(4)} + \frac{H_{in}}{6}cos\theta$$
$$-\frac{H_{out}}{6}sin\theta + \frac{4}{3}K_s cos2\theta \tag{27}$$

The fourth-order perturbation term can be represented using a 2×2 matrix, which consists of a row matrix and a column matrix, as shown below.

$$E(\varepsilon^4) = \varepsilon^3.F.\vec{\varepsilon} + \varepsilon^2.G.\varepsilon^2 \tag{28}$$

The elements of the 2×2 matrices *F* and *G* are defined as follows.

$$F_{11} = -\frac{1}{24}\left(JZ_1 - \frac{\omega}{4}\Phi_1\right) + \frac{\omega}{32}cos2\theta(8\Phi_0 + \Phi_1) - \frac{1}{3}cos2\theta D_1^{(2)} - \left(\frac{5}{3}cos^4\theta - 8cos^2\theta sin^2\theta + sin^4\theta\right)$$
$$D_1^{(4)} - \frac{H_{in}}{24}sin\theta - \frac{H_{out}}{24}cos\theta + \frac{N_d}{12\mu_0}$$
$$+\frac{4}{3}K_s sin2\theta \tag{29}$$

$$F_{12} = F_{21} = \frac{1}{6}\left(JZ_1 - \frac{\omega}{4}\Phi_1\right) + \frac{\omega}{8}cos2\theta\Phi_1$$
$$+\frac{N_d}{3\mu_0} \tag{30}$$

$$F_{22} = -\frac{1}{24}\left(JZ_1 - \frac{\omega}{4}\Phi_1\right) + \frac{\omega}{32}cos2\theta(8\Phi_0 + \Phi_1) - \frac{1}{3}cos2\theta D_2^{(2)} - \left(\frac{5}{3}cos^4\theta - 8cos^2\theta sin^2\theta + sin^4\theta\right)$$
$$D_2^{(4)} - \frac{H_{in}}{24}sin\theta - \frac{H_{out}}{24}cos\theta + \frac{N_d}{12\mu_0}$$
$$+\frac{4}{3}K_s sin2\theta \tag{31}$$

$$G_{11} = G_{22}$$
$$= 0 \tag{32}$$

$$G_{12} = G_{21} = -\frac{1}{8}\left(JZ_1 - \frac{\omega}{4}\Phi_1\right) + \frac{3\omega}{32}cos2\theta\Phi_1 + \frac{N_d}{4\mu_0} \tag{33}$$

As a result, the total magnetic energy expressed in equation (6) can be derived as follows.

$$E(\theta) = E_0 + \vec{\alpha}.\vec{\varepsilon} + \frac{1}{2}\vec{\varepsilon}.C.\vec{\varepsilon} + \varepsilon^2.\beta.\vec{\varepsilon} + \varepsilon^3.F.\vec{\varepsilon} + \varepsilon^2.G.\varepsilon^2 \tag{34}$$

To determine the minimum energy contribution from the second-order perturbed term.

$$\vec{\varepsilon} = -C^+.\alpha \tag{35}$$

The matrix C^+ represents the pseudo inverse of C and can be determined using the following method.

$$C.C^+ = 1 - \frac{E}{N} \tag{36}$$

In this case, E represents a matrix in which every element is defined as $E_{mn} = 1$, while I denote the identity matrix.

Therefore,

$$C_{11}^+ = C_{22}^+ = \frac{C_{21} + C_{22}}{2(C_{11}C_{22} - C_{21}^2)} \tag{37}$$

$$C_{12}^+ = C_{21}^+ = \frac{C_{21} + C_{22}}{2(C_{21}^2 - C_{11}C_{22})} \tag{38}$$

Therefore, from the matrix equation (35)

$$\varepsilon_1 = (\alpha_2 - \alpha_1)\, C_{11}^+ \tag{39}$$

$$\varepsilon_2 = (\alpha_2 - \alpha_1)\, C_{21}^+ \tag{40}$$

The total magnetic energy can be obtained by substituting ε into equation (34).

Results and Discussion

In this study, the graphs were generated for ferromagnetic thin films with an FCC lattice structure comprising two distinct spin layers. For FCC (001) oriented films, the selected parameters include $Z_0 = 4,\ Z_1 = 4,\ Z_2 = 0$ and $\Phi_0 = 9.0336,\ \Phi_1 = 1.4294$, as reported in previous studies [10-12]. These parameters define key structural and magnetic characteristics of FCC (001) thin films, significantly influencing the magnetic behavior and energy configurations analyzed in the simulations. Figure 1 displays a 3D plot illustrating the variation of energy as a function of angle and demagnetization energy for the parameter values $\frac{D_1^{(4)}}{\omega} = 5$ and $\frac{D_2^{(4)}}{\omega} = 10$. In this simulation, the remaining parameters are maintained at constant values: $\frac{H_{in}}{\omega} = \frac{H_{out}}{\omega} = \frac{N_d}{\mu_0\omega} = \frac{D_1^{(2)}}{\omega} = \frac{D_2^{(2)}}{\omega} = \frac{D_3^{(2)}}{\omega} = \frac{K_s}{\omega} = 10$. When compared to the second- and third-order perturbed models, the energy peaks in the angular direction are more closely packed (Samarasekara, 2007; Samarasekara & Mendoza, 2010; Samarasekara & De Silva, 2007; Samarasekara et al., 2009). Figure 2 represents a cross-sectional view of the 3D plot at a fixed angle, which can be obtained by rotating the visualization shown in Figure 1.

The graph indicates that energy maxima occur at $\frac{N_d}{\mu_0\omega} = 16, 26, 32, 52, 85, 91,$ with the most prominent peak observed at $\frac{N_d}{\mu_0\omega} = 91$. For the same crystal structure and the same number of spin layers, the total magnetic energy was observed to be on the order of 10^{51} when stress-induced parameters were employed (Farhan et al., 2023). However, in the present study, where demagnetization parameters are used instead, the total magnetic energy is found to be on the order of 10^{47}. This significant difference suggests that stress-induced effects contribute to a much higher energy state compared to demagnetization effects. The reduced energy in the demagnetization model indicates that the influence of magnetic dipole interactions and anisotropy is relatively weaker than the impact of internal stress-induced modifications. This comparison highlights the crucial role of different energy contributions in determining the overall magnetic behaviour of ferromagnetic thin films.

In this scenario, the total magnetic energy exceeds the value of 10^{13}, which was previously obtained when applying the fourth-order perturbed Heisenberg Hamiltonian with only spin exchange interaction and second-order anisotropy terms (Samarasekara & Ekanayake, 2021). This indicates that the inclusion of additional energy terms in the Heisenberg Hamiltonian contributes to an overall increase in the total magnetic energy.

Figure 3 illustrates the energy as a function of the angle, where the parameter $\frac{N_d}{\mu_0 \omega} = 91$. The graph reveals energy maxima at 2.45 and 5.058 radians, while energy minima occur at 0.5969 and 3.519 radians. Notably, the angle between the consecutive magnetic easy and hard axes is not exactly 90 degrees in this case. A similar observation is made when the stress-induced anisotropy constant is used as a parameter, maintaining the same spin layers and structure [8]. However, in the case of a simple cubic structure with the same spin layers and the same stress-induced anisotropy constant, the angle between consecutive magnetic easy and hard directions is exactly 90 degrees (Farhan & Samarasekara, 2022).

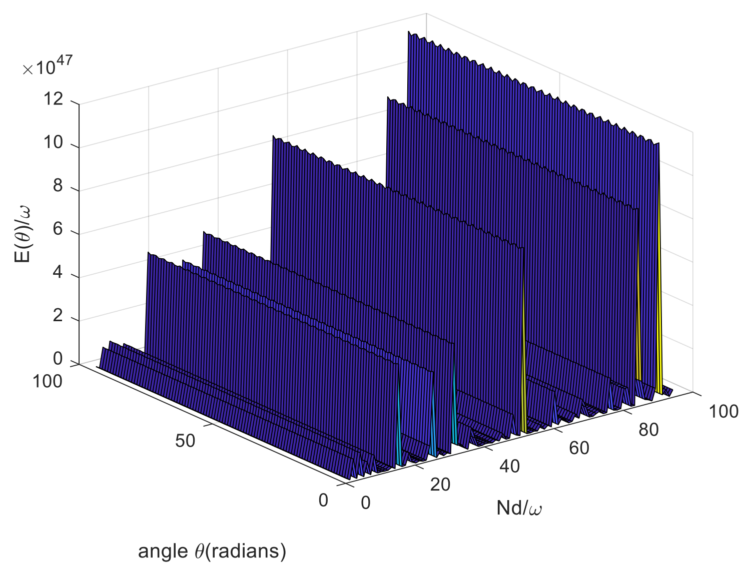

Figure 1: 3-D plot of energy versus angle and demagnetization energy for $\frac{D_1^{(4)}}{\omega} = 5$ and $\frac{D_2^{(4)}}{\omega} = 10$

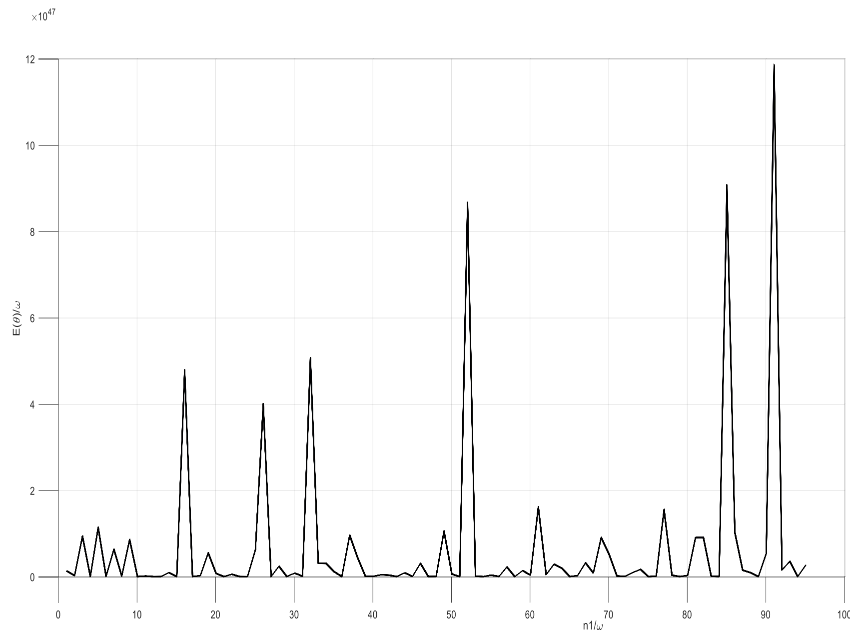

Figure 2: Graph of energy versus demagnetization energy

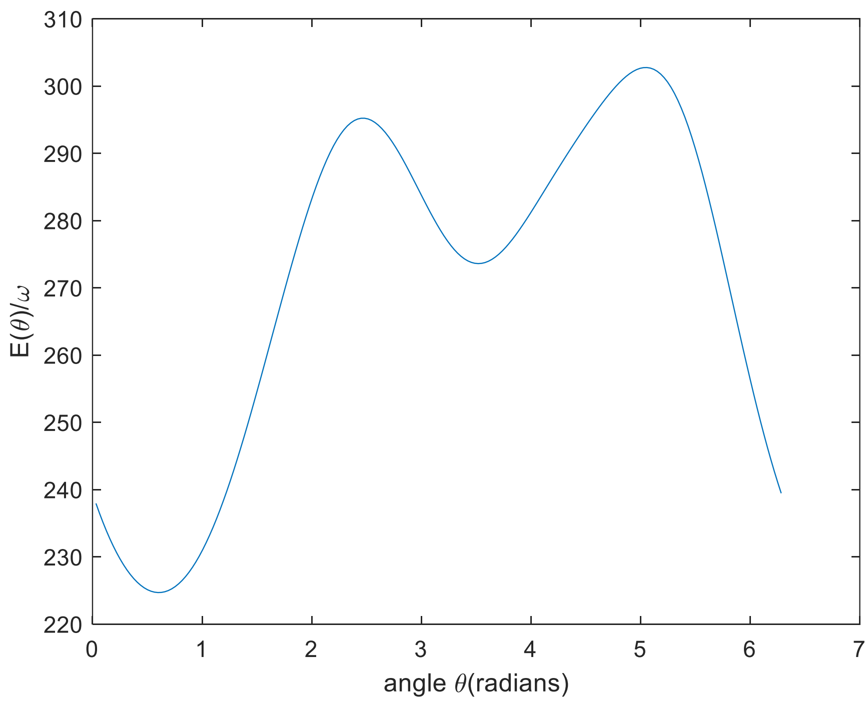

Figure 3: 2D graph of energy versus angle for $\frac{N_d}{\mu_0 \omega} = 91$.

Figure 4 presents a 3D plot of energy as a function of angle and demagnetization energy for $\frac{D_1^{(4)}}{\omega} = 10$ and $\frac{D_2^{(4)}}{\omega} = 5$, while keeping other parameters unchanged.

The graph highlights energy maxima at $\frac{N_d}{\mu_0 \omega} = 2, 6, 38, 61, 85$, with the most prominent peak occurring around $\frac{N_d}{\mu_0 \omega} = 2$, likely due to an optimal alignment of magnetic moments influenced by demagnetization effects. The total energy is on the order of 10^{46}, and a slight decrease from 10^{47} to 10^{46} is observed when the fourth-order anisotropy constants of the two spin layers are interchanged. This suggests that anisotropy distribution plays a role in stabilizing the energy configuration, subtly influencing the overall energy landscape and affecting the system's magnetic properties and stability.

Figure 5 presents a graph of energy as a function of angle at $\frac{N_d}{\mu_0 \omega} = 2$. The energy maxima occur at approximately 2.513 and 5.058 radians, while the minima are observed at 0.5341 and 3.487 radians. This indicates that the system has specific angular positions where energy is either at a peak or a trough, corresponding to stable and unstable magnetic orientations. Notably, the angle between the magnetic easy and hard directions deviates from the typical 90-degree separation, suggesting that the anisotropy effects are not purely uniaxial. Additionally, when compared to Figure 3, this 2D energy plot exhibits distinct spikes, which could be attributed to higher-order anisotropy contributions or variations in the energy landscape due to interactions between different anisotropy terms. These spikes indicate rapid energy changes at specific angles, possibly influencing the stability and dynamics of the system's magnetic configuration.

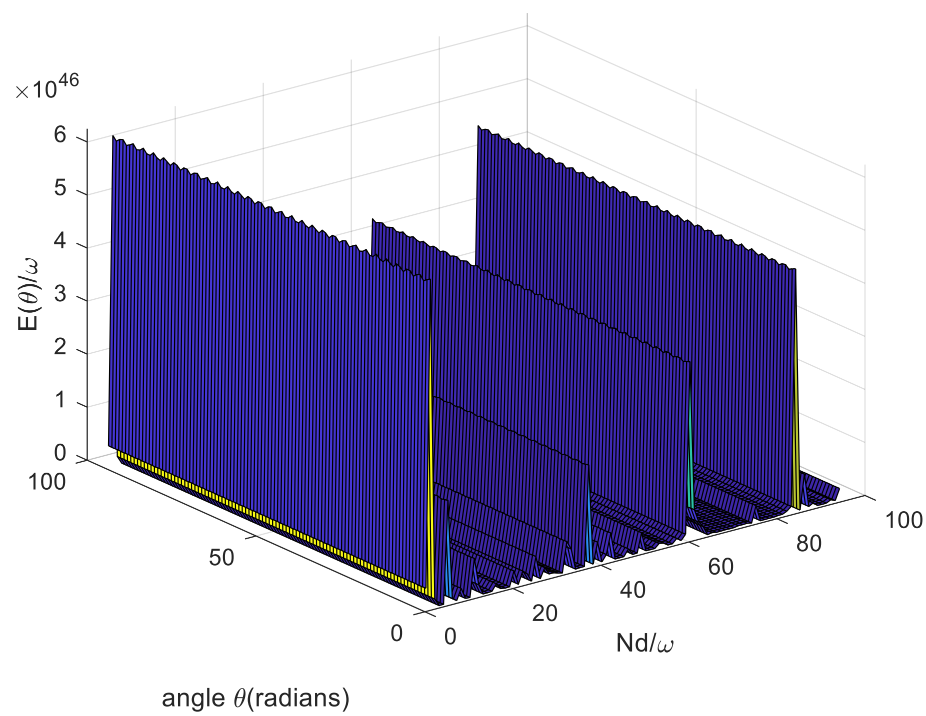

Figure 4: 3D plot of energy versus angle and demagnetization energy for $\frac{D_1^{(4)}}{\omega} = 10$ and $\frac{D_2^{(4)}}{\omega} = 5$

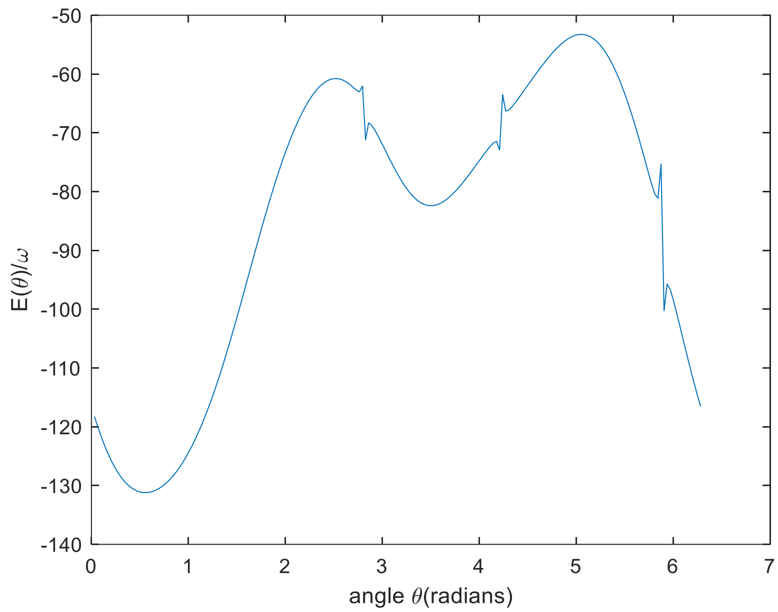

Figure 5: 2D graph of energy versus angle for $\frac{N_d}{\mu_0 \omega} = 2$.

Conclusion

This study investigates the magnetic properties of face-centered cubic (FCC) structured ferromagnetic thin films using the fourth-order perturbed Heisenberg Hamiltonian. By incorporating all seven key magnetic energy parameters, including spin exchange interactions, anisotropy constants, applied magnetic fields, stress-induced anisotropy, and demagnetization energy, we provide a comprehensive analysis of the energy landscape in FCC thin films. The MATLAB simulations, featuring both 3D and 2D plots, offer insights into the relationship between total magnetic energy, demagnetization effects, and azimuthal spin angle, highlighting the significance of higher-order anisotropy contributions.

The results demonstrate that the inclusion of fourth-order anisotropy terms significantly influences the magnetic energy distribution. The 3D energy plots reveal distinct energy maxima and minima, with the most prominent peaks occurring at specific values of the demagnetization parameter. Notably, the energy maxima at $\frac{N_d}{\mu_0 \omega} = 2, 6, 38, 61, 85$ suggest critical stable states in the system, with the strongest energy concentration around $\frac{N_d}{\mu_0 \omega} = 2$. Additionally, when comparing demagnetization energy effects with stress-induced parameters, the total energy is found to be lower in the demagnetization model, indicating that internal stress significantly enhances the system's energy state.

The angular dependence of energy extrema further reveals that the separation between magnetic easy and hard directions deviates from the conventional 90-degree alignment. This deviation, along with the observed energy spikes in the 2D energy plots, suggests the complex interplay of higher-order anisotropy and spin interactions. Moreover, interchanging the fourth-order anisotropy constants of the two spin layers results in a slight decrease in total energy, reinforcing the role of anisotropy distribution in system stability.

Overall, this study enhances the understanding of energy variations in FCC ferromagnetic thin films and underscores the importance of higher-order anisotropy effects. These findings contribute valuable insights for optimizing the magnetic properties of thin films in spintronic applications, data storage, and advanced magnetic materials. Future research could explore additional perturbation orders and extend the analysis to multilayered structures to further refine the theoretical framework for thin-film magnetism.

Conflicts of interest

The authors declare that there are no conflicts of interest.

Author contributions

M.S.M. Farhan conducted the literature review, prepared the graphs using MATLAB software, compared the findings with previous research, and drafted the original manuscript. P. Samarasekara provided expert guidance in the selection and formulation of the research topic, offered academic direction throughout the study, advised on the manuscript structure and content development, and critically reviewed and revised the manuscript.

References

Bentaleb M, Aouad El N, Saber M. Exact solution of the one-dimensional Ising model in a random oscillating magnetic field. Chinese Journal of Physics, 2002, 40: 307

Ernst A, Lueders M, Temmerman W, Szotek Z, van der Laan G. Theoretical study of magnetic layers of nickel on copper: dead or alive? Journal of Physics: Condensed Matter, 2000, 12: 5599–5606

Farhan M S M, Samarasekara P. A solution of fourth-order perturbed Heisenberg Hamiltonian with seven magnetic parameters. Journal of Nanoscience and Nanoengineering Applications, 2022, 12(1): 1–12

Farhan M S M, Samarasekara P. Fourth-order perturbed Heisenberg Hamiltonian with seven magnetic parameters of BCC structured ferromagnetic ultrathin films. GESJ: Physics, 2022, 1(26): 29–45

Farhan M S M, Karunarathna M A A, Samarasekara P. Investigation of magnetic properties of ferromagnetic thin films with three spin layers using fourth-order perturbed Heisenberg Hamiltonian. Ceylon Journal of Science, 2023, 52(2): 133–142

Farhan M S M, Samarasekara P, Abeyratne M K. FCC structured ferromagnetic ultra-thin films with two spin layers described by fourth order perturbed Heisenberg Hamiltonian with all seven parameters. GESJ: Physics, 2023, 1(28): 17–25

Farhan M S M, Karunarathna M A A, Samarasekara P. Exploring magnetic anisotropy in BCC-structured ferromagnetic thin films with three spin layers using the fourth order perturbed Heisenberg Hamiltonian. GESJ: Physics, 2024, 1(30): 6–19

Hucht A, Usadel K D. Reorientation transition of ultrathin ferromagnetic films. Physical Review B, 1997, 55: 12309

Hucht A, Usadel K D. Theory of the spin reorientation transition of ultra-thin ferromagnetic films. Journal of Magnetism and Magnetic Materials, 1999, 203(1): 88–90

Samarasekara P. Influence of third order perturbation on Heisenberg Hamiltonian of thick ferromagnetic films. Electronic Journal of Theoretical Physics, 2008, 5(17): 227–236

Samarasekara P, Mendoza W A. Effect of third order perturbation on Heisenberg Hamiltonian for non-oriented ultra-thin ferromagnetic films. Electronic Journal of Theoretical Physics, 2010, 7(24): 197–210

Samarasekara P, De Silva S N P. Heisenberg Hamiltonian solution of thick ferromagnetic films with second order perturbation. Chinese Journal of Physics, 2007, 45(2-I): 142–150

Samarasekara P, Abeyratne M K, Dehipawalage S. Heisenberg Hamiltonian with second order perturbation for spinel ferrite thin films. Electronic Journal of Theoretical Physics, 2009, 6(20): 345

Samarasekara P, Warnakulasooriya B I. Five layered FCC ferromagnetic films as described by modified second order perturbed Heisenberg Hamiltonian. Journal of Science of the University of Kelaniya Sri Lanka, 2016, 11: 11–21

Samarasekara P, Saparamadu U. In-plane oriented strontium ferrite thin films described by spin reorientation. Research & Reviews: Journal of Physics – STM Journals, 2013, 2(2): 12–16

Samarasekara P, Ekanayake E M P. Fourth order perturbed Heisenberg Hamiltonian of FCC structured ferromagnetic ultra-thin films. GESJ: Physics, 2021, 1(25): 19–29

Spisak D, Hafner J. Theoretical study of FeCo/W (110) surface alloys. Journal of Magnetism and Magnetic Materials, 2005, 286: 386–389

Usadel K D, Hucht A. Anisotropy of ultrathin ferromagnetic films and the spin reorientation transition. Physical Review B, 2002, 66: 024419

Zhao D, Liu F, Huber D L, Lagally M G. Step-induced magnetic-hysteresis anisotropy in ferromagnetic thin films. Journal of Applied Physics, 2002, 91: 3150–3153